

Identification of sand sources and transport pathways at the Kelso Dunes, California, using thermal infrared remote sensing

Michael S. Ramsey* }
Philip R. Christensen } Department of Geology, Arizona State University, Tempe, Arizona 85287-1404
Nicholas Lancaster } Desert Research Institute, 7010 Dandini Boulevard, Reno, Nevada 89512
Douglas A. Howard† } Department of Geology, Arizona State University, Tempe, Arizona 85287-1404

ABSTRACT

The Kelso dune field is located in the eastern Mojave Desert, California, at the terminus of a sand-transport pathway, which has its primary source at the Mojave River Wash 50 km to the west. Initial examination of 1984 airborne thermal infrared multispectral scanner (TIMS) data showed significant spectral variations that indicate potential mineralogic heterogeneities within the active dunes. This result prompted the collection of a suite of 48 sand samples in 1990, and the acquiring of new TIMS data in 1995. This new data set was used to test a newly developed linear spectral retrieval algorithm in conjunction with a spectral library of end-member minerals. Results of this analysis produced images of end-member minerals that showed marked variations within the dunes. In addition, standard petrographic techniques revealed that the dunes contain mineralogic variations and were much less quartz rich (~42%) than previously reported (~70%–90%). Point-count results agreed with the spectral data to within an average of 5.3% for TIMS-derived and 3.1% for laboratory-derived mineralogic abundances. High concentrations of several of the end-member minerals on the surrounding alluvial fans indicate a potential nearby source for these minerals. Most evident is the presence of potassium feldspar from the fan that emanates from the Providence Mountains east of the dunes. This previously unidentified potential sand input is not visible with other remote sensing techniques and was confirmed with additional field sampling. Much of the quartz and some plagioclase feldspar, however, appear to

have been transported from the Mojave River Wash source as previously reported. This study also validates the potential of using thermal remote sensing from future satellite-based instruments to globally monitor desert fringe areas susceptible to the changing conditions of sand encroachment.

INTRODUCTION

In arid regions throughout the world, the geologic processes of sediment weathering, transport, and deposition are constantly ongoing within active sand-transport pathways. The analysis of dune-field composition and movement is critical for the interpretation of past climatic conditions, local geology, and future desertification potential. This type of comprehensive study typically involves many years of data collection, mapping, and sample classification (e.g., Sharp, 1966; Muhs et al., 1995). Although detailed field studies of this nature are extremely valuable, their magnitude and temporal dependency can clearly lead to generalizations in both the source and amount of mineralogic heterogeneity within a large dune field.

The use of remote sensing over the past several decades as a tool to study dynamic features such as dunes has given the geologist a synoptic view of entire eolian systems as well as their sediment sources (Breed and Grow, 1979; Blount et al., 1990; Edgett et al., 1995). In addition, the ability to examine changes over time allows for the extrapolation of past climatic regimes and the monitoring of marginal areas susceptible to future desertification (Otterman, 1981; Leonidov, 1989; Tucker et al., 1994). The first stage in studies such as these is the classification of image-wide units such as vegetation, sand, and rock outcrops. However, to approach the level of detail needed to track sediment transport into the dune field and

assess the degree of weathering, information below the scale of the image resolution, such as the surface mineralogy and abundance, are critical. The accurate retrieval of this subpixel information from multispectral remote sensing data requires the knowledge of how the radiated energy from each surface component interacts as well as a model to separate that mixed energy for each end member (spectral deconvolution). Deconvolution or retrieval models, whether linear or not, rely on the input of end-member spectra to perform a best fit to the unknown (mixed) spectrum. The choice of a linear or nonlinear model depends on the physics of the matter-energy interaction, which are primarily functions of the wavelength region examined and the particle size of the surface materials.

Several authors have used remote sensing in the visible–near infrared (VNIR) region (0.4–2.5 μm) to study alluvial fans, sand seas, and dune fields (Shipman and Adams, 1987; Blount et al., 1990; Paisley et al., 1991). However, the results of these studies were limited due to the complications of VNIR remote sensing, which include nonlinear mixing (Hapke, 1981; Clark, 1983; Johnson et al., 1992), and the inability to accurately distinguish many silicate minerals because of their generally featureless spectra (Blount et al., 1990). The nonlinear mixing of reflected energy in this wavelength region results from particle size effects, which alter the spectral features (Hapke, 1981; Mustard and Pieters, 1989). In addition, and even more significant, is that most rock-forming minerals in the VNIR are relatively transparent, favoring nonlinear volume scattering over simple reflection (Johnson et al., 1992). Mineral identification and mapping of alluvial material using data from the thermal infrared (TIR) region (8–12 μm) is simplified due to the linear nature of emitted energy in most cases (Thomson and Salisbury, 1993; Ramsey et al., 1994; Ramsey and Christensen,

*E-mail: ramsey@elwood.la.asu.edu.

†Present address: ERDAS Inc., 2801 Buford Highway N.E., Atlanta, Georgia 30329.

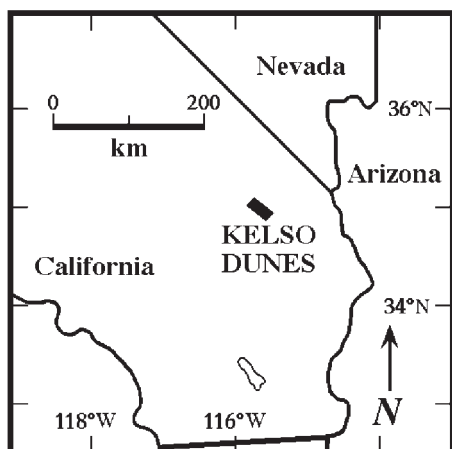


Figure 1. Location map of southern California showing the Kelso Dunes. The rectangle indicates the approximate size and orientation of the airborne data displayed in Figure 2.

1998). Even in this wavelength region, the assumption of linearity becomes invalid for non-isothermal surfaces or very fine grained materials (Gillespie, 1992; Ramsey and Christensen, 1998). Dunes, however, provide an excellent target for testing linear algorithms because they generally lack thermal shadows and consist of larger particles, free of fines. Furthermore, every major dune-forming mineral (silicates, carbonates, and sulfates) has diagnostic absorption features in the 8–12 μm wavelength region, making detection much easier. In the past, spectral deconvolution using TIR data has been attempted on both volcanoclastic, mafic dunes (Edgett et al., 1995) and more quartz-rich sands (Ramsey et al., 1993, 1994). Results of both studies clearly identified surface mineralogy as well as mixing patterns of the components. The use of thermal infrared remote sensing can therefore be used to more accurately identify dune composition and sediment transport into the system. With this knowledge, the commonly complex history of a particular dune field like Kelso becomes easier to decipher.

In addition to a more detailed exploration of the geology of the Kelso Dunes (Fig. 1), another main focus of this work is to vigorously test the linear retrieval algorithm, using library mineral spectra as end members to deconvolve the thermal infrared multispectral scanner (TIMS) data. The 1995 data set traverses the primary north-west-southeast sand-transportation pathway from the Mojave River Wash into the dunes (Fig. 2) and contains far less microphonic noise than the original 1984 imagery (Barbera, 1989). Microphonic noise is commonly caused by electronic interference during data collection, producing scan line striping or a “venetian blind” effect in the images. This noise can have an adverse effect



Figure 2. NS001 airborne scanner (Landsat Thematic Mapper simulator) visible image of the primary Kelso Dune sand-transport pathway from the Mojave River wash. The data, acquired concurrently with the thermal infrared multispectral scanner (TIMS) imagery in 1995, show the Kelso Dunes, Devils Playground, and surrounding mountain ranges. The white dashed region denotes the area analyzed in detail using the TIMS (see Figs. 8 and 13). The only current actively saltating sand occurs along the three main linear ridges of the Kelso Dunes and the small crescentic dunes in the western Devils Playground (south of Soda Lake playa). The prevailing east-southeast wind direction is opposed by topographically controlled westerly winds that keep the main core of the Kelso Dunes stationary, overlapping the alluvial fans of the Granite and Providence Mountains.

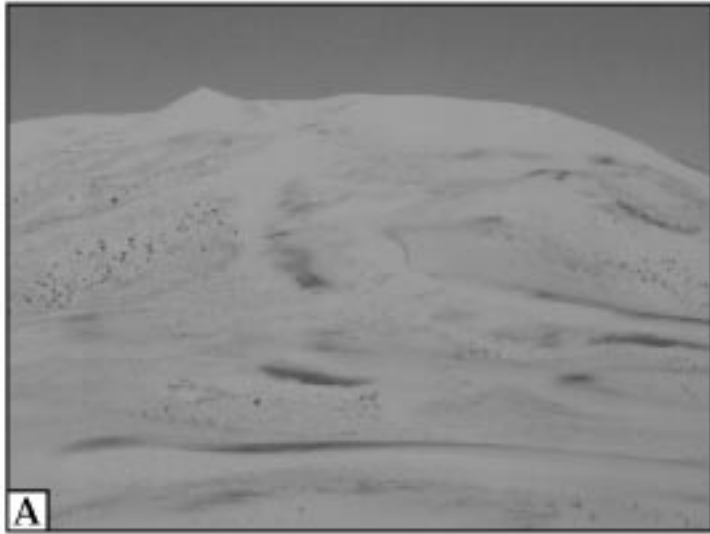
on the results of image analysis techniques such as linear deconvolution. The new data were also subjected to model iterations using a larger suite of mineral end members, many of which were not present in the dune sands. Such an analysis provides a test of the model’s ability not only to deconvolve the spectra, but to accurately identify which minerals are likely present in the scene. Model-predicted modes were compared against petrographically derived modes from collected

samples. Regions of potential local sediment input and higher model errors were also investigated further with new field work.

GEOLOGY OF THE KELSO DUNES REGION

The Kelso Dunes are located in the eastern Mojave Desert, California, ~95 km west of the California-Arizona border (Fig. 1). The rocks that

Figure 3. Photographs of the Kelso Dunes area. (A) Crest of the southernmost linear ridge (view to the west; ridge height ≈ 120 m). This area of actively saltating sand is marked by a discontinuous veneer of magnetite lag and sparse vegetation ($<1\%$). (B) Typical vegetation pattern on the Providence Mountain alluvial fan (view to the east; cholla cactus in foreground ≈ 1 m). The ridge line consists primarily of Mesozoic quartz monzonite and Tertiary rhyolite and is the dominant source of much of the potassium feldspar on the fan and within the dunes. (C) View of the quartz monzonite showing the large (1 cm), easily weathered potassium-feldspar phenocrysts.



compose the mountain ranges surrounding the dunes range from metamorphosed Proterozoic island-arc remnants, which form much of the southern Kelso Mountains, to Paleozoic metasedimentary rocks that compose the majority of the northern Granite and portions of the Providence Mountains, to Tertiary rhyolite in the Providence Mountains (Jennings, 1961; Bishop, 1963). Also present is the Teutonia batholith, the dominant intrusive rock in the eastern Mojave Desert. It was emplaced throughout later Mesozoic time, and ranges compositionally from monzonite to granodiorite (Beckerman et al., 1982). In the vicinity of the dunes, the batholith is primarily a quartz monzonite (McDonald and McFadden, 1994), weathering to 1 cm grus of alkali feldspar and plagioclase with lesser amounts of quartz.

The Kelso dune field covers more than 100 km² and is contained within a topographic basin bounded by the Kelso, Providence, Granite, and Bristol Mountains to the north, east, south, and west, respectively (Fig. 2). It encroaches upon the alluvial fans that extend northwest from the Providence and Granite Mountains (McDonald and McFadden, 1994). The dune field consists of a core region of active sand containing three parallel linear ridges as high as 170 m (Fig. 3A). However, the overall westward migration of the dunes is kept to a minimum by topographically controlled winds, which oppose the prevailing westerly wind direction (Sharp, 1966; Reheis and Kihl, 1995).

Surrounding the region of active crescentic and complex linear dunes on the west, north, and east sides are areas of inactive 3–15-m-high vegetated dunes and stabilized sand sheets (Sharp, 1966; Yeend et al., 1984; Lancaster, 1990). The vegetation cover consists primarily of galleta grass that can cover 20% of the dune surfaces. The areal abundance and number of plant species increase on the adjacent alluvial fans to include a variety of small cactus, bushes (mainly creosote), and other grasses (Fig. 3B). Under the current cli-

TABLE 1. SAND MINERALOGY OF THE KELSO DUNES

Mineral	Sharp (1966) (%)	Paisley et al. (1991) (%)	This study (%)
Quartz	70–80	90.0	42.0
Feldspar	10–30	N.D.	N.D.
Plagioclase	N.D.*	N.D.	29.0
Microcline	N.D.	N.D.	21.0
Opaque	5–10	N.D.	5.8
Other	3–10	10.0	2.2

*N.D. = not determined.

mate regime active sand transport is limited, and no sand from the Mojave River Wash appears to reach the main dune mass (Smith, 1984). During these periods of marginal eolian activity, when long-distance transport is limited, local sediment may provide the primary source of new material into the dunes (Ramsey and Christensen, 1997).

The Kelso dune field was formed in a much more arid climate than present; the age of activity was initially estimated to be older than 100 ka (Yeend et al., 1984). However, dating using infrared stimulated luminescence places the age of the dunes between 40 ± 17 yr (modern surface sample) and 10.41 ± 0.89 ka (the basal parts of vegetated dunes); three distinct periods of major eolian activity occurred before 4.0 ka, ca. 1.5 ka, and 0.4–0.8 ka (Edwards, 1993; Wintle et al., 1994; Clarke, 1994). Dates on the surrounding sand ramps of the Devils Playground and sand sheets southeast of Kelso indicate that eolian activity was occurring as early as 16–20 ka (Clarke, 1994; Rendell and Sheffer, 1996). Most of the dune field is relatively inactive at present; the majority of sand movement is restricted to the tops of the three northeast-trending linear ridges (Paisley et al., 1991). Dunes in this region appear to undergo very rapid change, as indicated by a luminescence age of 64 ± 22 yr for an 8-m-deep sample (Edwards, 1993).

Previous investigations have studied the dunes in detail, reporting on the sand mineralogy and sources. They have estimated that the dunes are about 70% (Sharp, 1966) to 90% (Paisley et al., 1991) quartz, with lesser amounts of undifferentiated feldspar, in addition to minor opaque and mafic minerals (Table 1). The sand composition has been attributed to the both the source geology and transport distance (Sharp, 1966; Lancaster, 1993).

METHODS

Sample Collection and Analysis

The original TIMS data for the Kelso region of the Mojave Desert were acquired on September 7, 1984, with a ground resolution at nadir of ~ 17 m/pixel (Barbera, 1989). A decorrelation stretch of the data showed significant

color variations throughout the main part of the dune field, indicating spectral and therefore compositional differences (Fig. 4). The decorrelation technique, explained in detail by Gillespie et al. (1986), is a transformation of the original data that highlights compositional information as color variations and surface temperature changes (which correlate to topography) as intensity (brightness) variations. A surface having a constant mineralogic composition and in partial shadow (cooler) would appear as a single color in the decorrelation stretch image, the bright areas indicating the nonshaded (warmer) regions. This image-processing tool does not separate temperature from emissivity, but does allow the effect of each to be distinguished visually, and greatly improves the color contrast of the highly correlated TIMS data. These color variations prompted an image verification and sample-collection trip in 1990 by P. Christensen, N. Lancaster, and others (1993, personal commun.), during which 48 bulk samples were collected along a 9.5 km north-south traverse of the active dune field (Fig. 4). These samples represented different image color units as well as varying positions on individual dunes (crest versus swale). In addition, magnetite surface-lag deposits and nondune areas (Cottonwood Wash and the alluvial fans of the Granite Mountains) were sampled.

Laboratory thermal emission spectra were acquired for the entire suite of samples; 13 of 48 were chosen for further petrographic analyses to determine the modal abundances and to verify the results of the emission spectroscopy. The bulk sand was initially split into 20 g subsamples (Cadle, 1955). From each sample, ~ 5 g were retained for spectral analysis and the remainder embedded in epoxy with a potassium feldspar stain, and thin sections prepared. The choice of thin section samples (K1–K42 in Fig. 4) was based on color variations within the TIMS scene. However, six of these (K1–K6) were from a small (<0.5 km²), mineralogically similar region of the dune field and served as a consistency check on the precision of the point-count analysis versus results derived from the emissivity spectra.

At least 200 unbiased grains per sample were

counted using a technique described by Jones (1987). Mineralogy, particle diameters, and grain shape were noted throughout the procedure. Under plain light (Fig. 5A) potassium feldspar and opaque and mafic minerals can be readily identified. However, the rounded, similar-sized quartz and plagioclase grains are nearly indistinguishable. Even under crossed polars (Fig. 5B) these two are not always separable due to the commonly obscured or absent feldspar twinning. In the case of an identification uncertainty, an attempt was made to acquire the optic-axis figure for that mineral grain. This level of detailed petrographic analysis had not been attempted in the past for the Kelso sands. In contrast, a similar analysis conducted using only high-powered magnification, or under plain light in the case of thin sections, would underrepresent plagioclase feldspar with respect to quartz. This factor is the probable cause of the discrepancy between this work and past studies (Sharp, 1966; Yeend et al., 1984; Paisley et al., 1991).

Sodium-polytungstate heavy liquid separation was used to physically separate the primary end-member minerals (quartz, feldspar, and magnetite) for the remaining sample portion not used in thin-section preparation. This separation was performed in an attempt to use the exact dune-sand composition as end members for the spectral deconvolution. However, it was not entirely successful due to the overlap in the density of quartz and feldspar, as well as the inability to separate potassium feldspar and plagioclase. This was confirmed by the presence of spectral features from each mineral visible in the spectrum of the other mineral separate. Following several separation iterations, the emission spectra of the purest samples of quartz and feldspar separates were collected to judge the magnitude of the remaining contamination (Fig. 6). These spectra were treated as mixed samples and subjected to the same linear deconvolution using spectra of library minerals as end members. The results showed a 6.5% quartz contamination in the feldspar separate and a 34.1% feldspar contamination in the quartz. This contamination, together with the accurate results of using the library minerals as end members, prompted the abandonment of further separation attempts. Library-derived end members also provide a much more realistic scenario for future image analysis in more remote regions where sample collection would be impossible.

The thermal emission spectrometer spectral library consists of ~ 200 minerals, each meticulously analyzed for purity. Three of the four mineral end members (quartz, oligoclase, microcline) were taken directly from the spectral library (Fig. 7). The temporally variant existence of the magnetite surface-lag deposits and the high percentage of



Figure 4. Decorrelation stretch image of the 1984 thermal infrared multispectral scanner (TIMS) data with bands 5 (10.7 μm), 3 (9.2 μm), and 1 (8.4 μm) in red, green, and blue, respectively (see Barbera [1989] for a description of the data). Sand sample sites are shown as white diamonds; numbered samples were used for petrographic analysis. The color changes in the image indicate mineralogic variations, whereas brightness differences show surface temperature changes (see text). Close examination reveals a horizontal “venetian blind” striping that is caused by microphonic noise present in the raw data. This noise is exaggerated upon data transformation using techniques such as the decorrelation stretch and linear retrieval. Together with the limited areal coverage of the surrounding alluvial surfaces, this prompted new TIMS data to be collected in 1995 (Fig. 8).

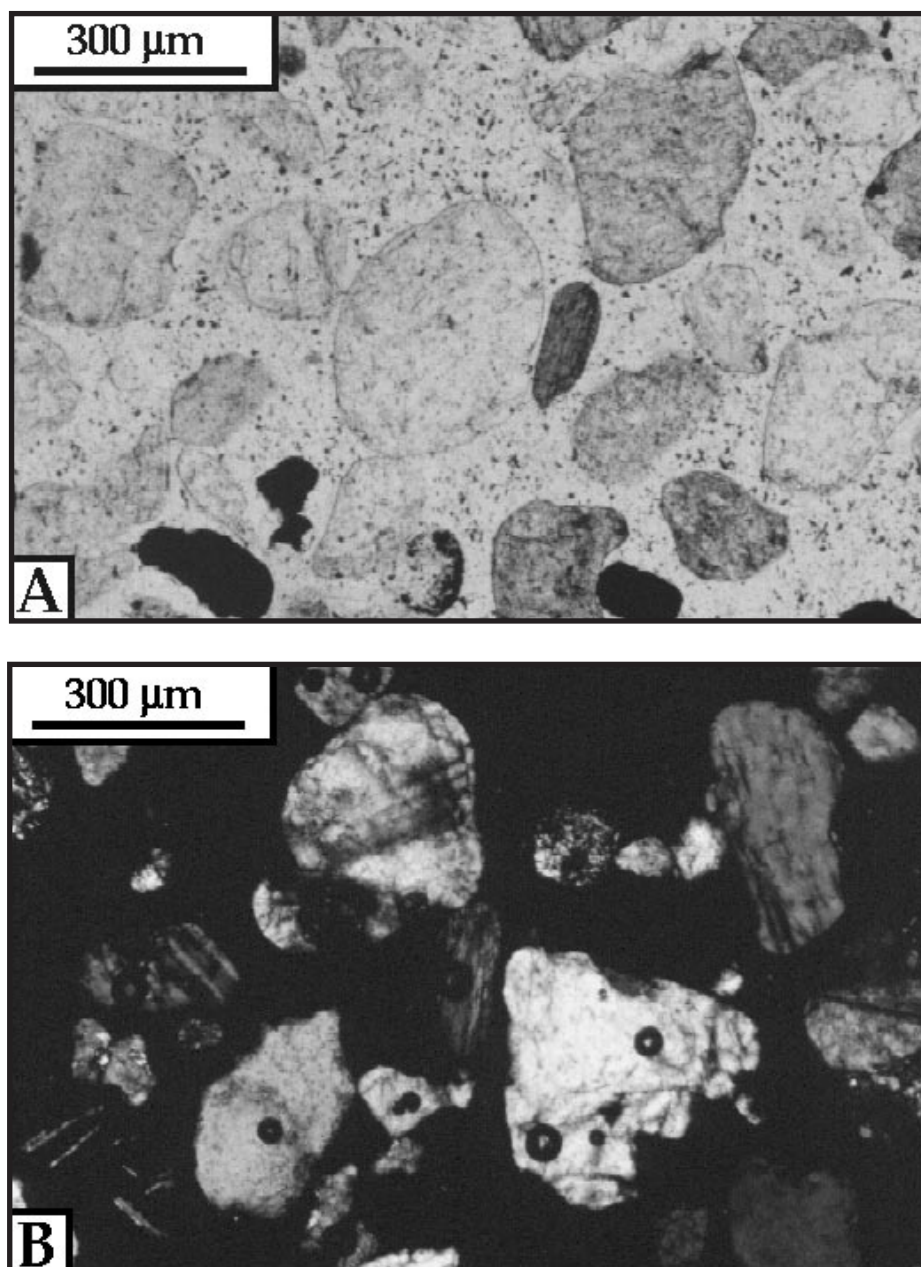


Figure 5. Photomicrographs of the Kelso Dunes sand samples. (A) Sample K1c taken in plain light with potassium-feldspar stain. The large rounded plagioclase grain in the center is difficult to distinguish mineralogically from the surrounding subrounded particles of quartz. Smaller mafic grains of hornblende (center) and magnetite (bottom) are present in <4% quantities throughout most of the dune field. (B) Sample K42c taken with crossed polarizers. Even with polarization, the common parallel twinning characteristic of plagioclase feldspar is not always evident (cf. the large white plagioclase grain in the lower right with the grayish quartz grain in the lower left). In such cases, an optic-axis figure was taken if possible to accurately identify quartz.

clay in some low-lying samples made these minerals strong candidates as the fourth end member. However, examination of the spectra of magnetite and fine-grained sodium-montmorillonite showed them to be nearly identical over the 8–12 μm

range, especially where considering the degradation to six points to match the TIMS image channels. Due to the spectral similarity, neither mineral would be differentiated by the linear retrieval algorithm. Therefore, a clay plus magnetite end mem-

ber was used, formed by numerically averaging the spectrum of each. The laboratory emission spectra of all 48 bulk samples were deconvolved using the four end members in Figure 7. Model results for the 13 thin-sectioned samples were then compared to the mineral percentages derived from the point-count analysis.

1995 Data Acquisition and Image Processing

New TIMS data were acquired at 13:20 local time on June 12, 1995, to trace sand transport across the Devils Playground and examine potential sediment sources to the northwest of the main dune Kelso field. Two lines were flown, beginning at the Providence Mountains, extending northwestward across the Devils Playground, and terminating 50 km to the west at the Mojave River Wash (Fig. 2). Aerial photographs, NS001 scanner (Landsat Thematic Mapper simulator) data, and TIMS data were acquired simultaneously from the NASA C130 aircraft at an altitude of 8535 m above ground level. This altitude was near the maximum for the C130 and resulted in an image resolution of 21.3 m/pixel at nadir. The high altitude produced the largest possible areal coverage at the sacrifice of small-scale details. At the time of the over flights, moderate to high humidity levels (~25%) were present in the area. Because atmospheric path radiance increases with higher altitudes and water-vapor percentage, accurate correction and removal of the upwelling and downwelling atmospheric energy are generally more difficult using radiative transfer models. These models use averaged atmospheric profiles and make no corrections for the topographic variability within the scene.

For this study a small segment of one TIMS line, which covered the dunes, surrounding alluvial fans, and the eastern sand sheets, was used (Fig. 2). The data were calibrated to radiance-at-sensor and geometrically corrected for the scan angle of the instrument. Atmospheric path radiance was removed using the MODTRAN atmospheric model (Berke et al., 1989) with the standard midlatitude summer correction. Due to the side-scanning configuration of the TIMS instrument, pixels on the edge of the image contain nearly 20% more atmospheric energy than those at nadir. Even after the MODTRAN correction, this geometric effect causes a nonuniform color aberration on the image edges. However, no attempt was made to further correct the data at this stage because the primary surfaces of interest were centered in the image, where water-column abundance and edge effects are minimized. Continued nonstandard data manipulation (Barbera, 1989; Edgett and Anderson, 1995) may adversely skew the results of the retrieval algorithm by al-

tering the spectral features of the units nonuniformly throughout the scene.

The atmospherically corrected data were then separated into six emissivity and one brightness temperature image (Fig. 8) with the technique described by Realmuto (1990). The Planck equation, which describes the behavior of emitted thermal energy, is underdetermined with respect to physical measurements of temperature and radiance. For example, the TIMS records six radiance values, which contain seven unknowns (one emissivity value for each of the six channels and one ground temperature). An assumption of one of the emissivities is typically made to solve for the remaining unknowns. For this study a maximum assumed emissivity of 0.973, derived from the TIMS band 6 (11.7 μm) average of the laboratory spectra of the 48 samples, was used. Once separated from the temperature, the six emissivity images served as inputs into the linear retrieval model in conjunction with the library end-member spectra degraded to six points using the calibrated spectral band passes for the TIMS instrument (Realmuto et al., 1995).

The assumption of linear mixing of thermal radiant energy is valid due to the fact that most geologically significant minerals have very high absorption coefficients in the TIR, resulting in a much shorter path length and less scattering for the emitted photons. As a result, the majority of the energy detected by a sensor has interacted with only one surface particle. Upon mixing, the spectral features from surface particles are retained in proportion to their areal extent. Therefore, assuming that the pure mineral spectra (end members) are known, thermal infrared spectra can be linearly deconvolved in order to ascertain mineralogic percentages. This deconvolution has been performed here by using a least-squares approach that results in one image per end member along with a root-mean-squared (RMS) error image. Whereas the end-member images can be used to visualize spatial patterns and mixing, the RMS image becomes invaluable in order to assess the quality of a given algorithm iteration. The mineral end-member images were compared to the deconvolution results of the laboratory spectra as well as the point count modal values. False color composites of three of the end-member images indicated regions of complex mixing and sediment inputs. On the basis of these images, several field areas were revisited and new samples were collected.

For the TIMS portion of this study the algorithm was not given access to only the four primary mineral end members. Rather, it was run several times using the blind end-member approach described by Ramsey and Christensen (1998). This technique is a user-independent selection, where the algorithm is given access to 15 of the most likely mineral end-member spectra. It

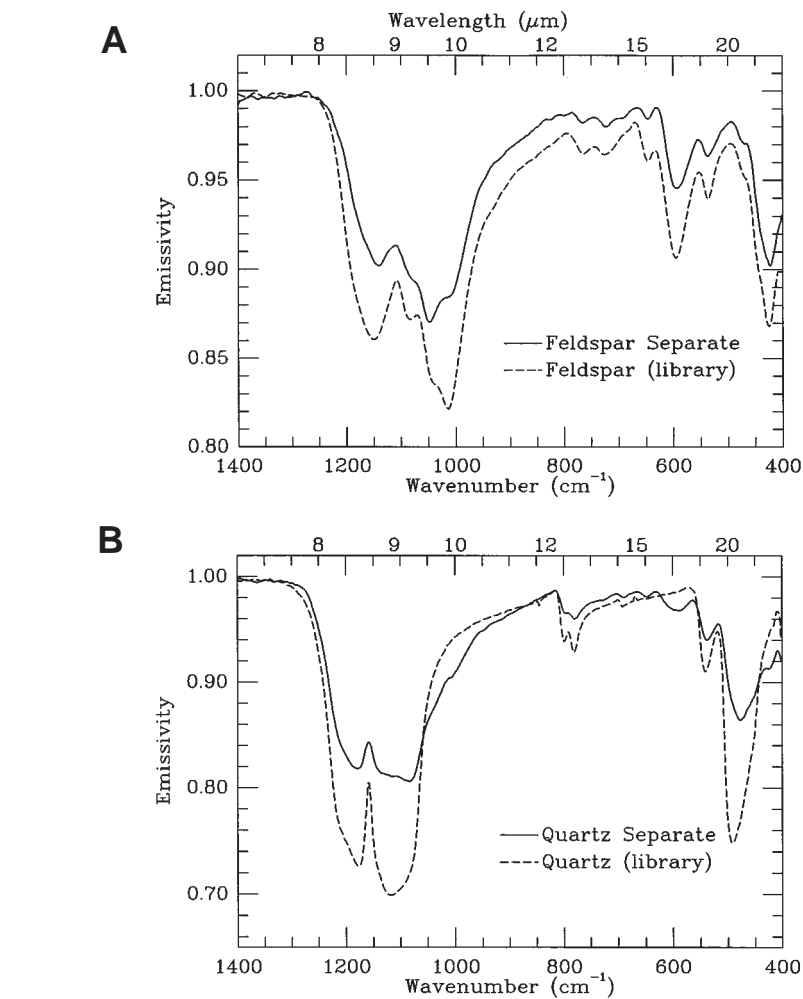


Figure 6. (A) Feldspar. (B) Quartz. Emission spectra of the best-case separation of feldspar and quartz derived from the heavy-liquid technique. Each spectrum is plotted with a pure library end member for comparison. Contamination of each spectrum by the other mineral is visible in the spectral features being most evident in the quartz spectrum, where 34% feldspar still remained. This contamination shows as a reduction in contrast of the primary absorption band at 1150 cm^{-1} , the development of band shoulder at 1000 cm^{-1} , and several smaller absorption bands between 600 cm^{-1} and 700 cm^{-1} . Due to the subtle density contrast of these minerals, further separation was deemed impossible (see text).

is allowed to iterate to a suite of end members with the lowest RMS error, and in a majority of the scene, the four primary minerals identified using petrography were also chosen by the model.

The original sample sites from 1990, plotted on the 1984 decorrelation images (Fig. 4), were located on the 1995 images and the end-member percentages were extracted. The locations were pinpointed by geometrically rotating and warping the 1984 data to the 1995 image. The slight uncertainty in this registration technique and the lower spatial resolution of the new data set constrained the 1990 sample locations to within at best two pixels on the 1995 image. To minimize this slight error, all emissivity and end-member

percentage values extracted from the data were an average of nine pixels (one pixel removed in each direction from the most likely sample site).

The final stage of this study was to revisit the site, collecting samples along an east-west traverse of the Providence Mountain fan. This was prompted by the identification of a strong microcline occurrence in the deconvolution images in this area (see Results). Sampling was performed from the active dunes eastward up the fan to the Providence Mountains to confirm a source for this apparent contribution to the dunes. The monzonite in the vicinity contains large (>1 cm) phenocrysts of potassium feldspar (Fig. 3C), which weathers to a grus at the base of the outcrops.

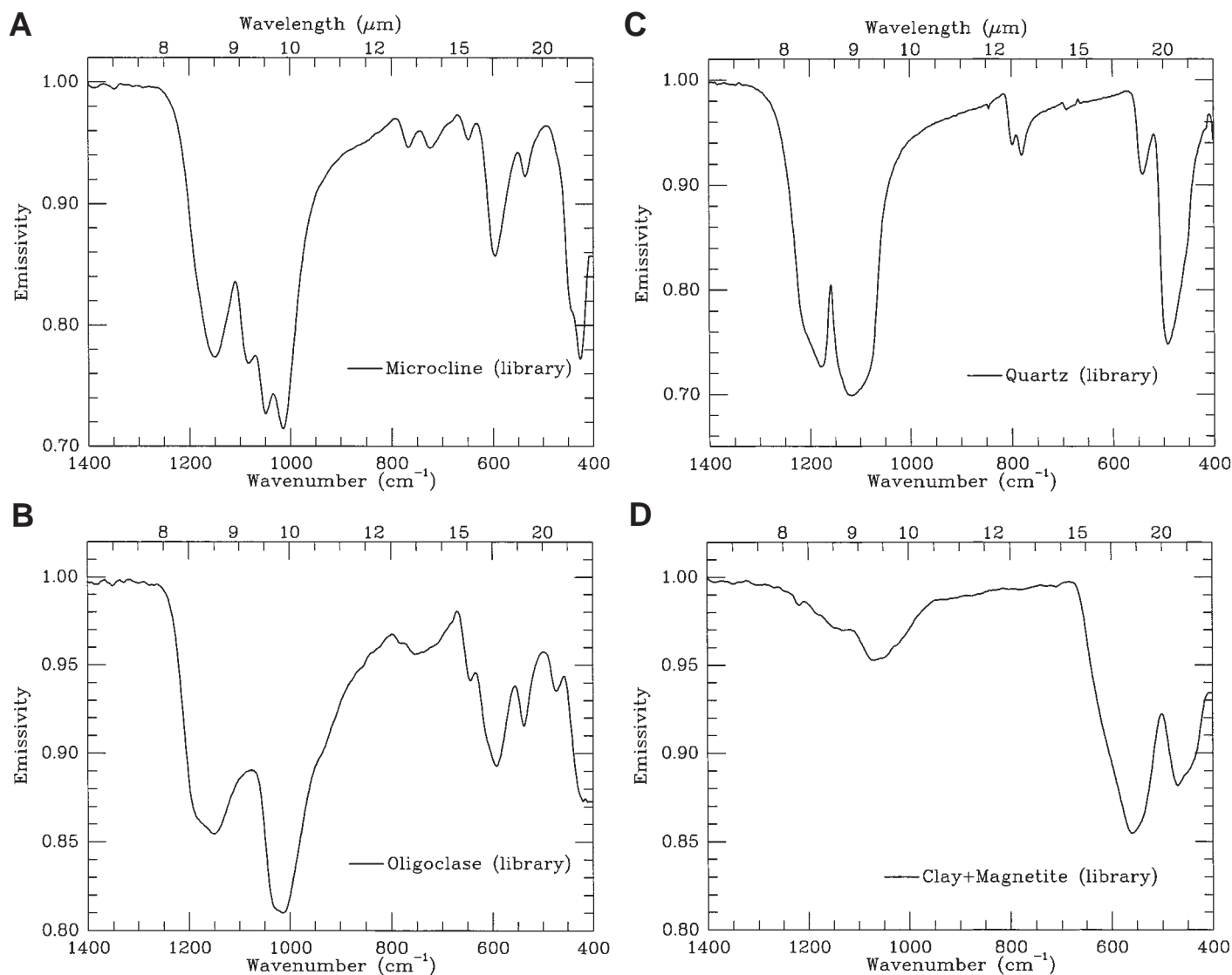


Figure 7. (A) Microcline. (B) Oligoclase. (C) Quartz. (D) Clay + magnetite. Library emission spectra used as end members for this study (average grain diameter = 500 μm). The large absorption bands between 1200 cm^{-1} and 1000 cm^{-1} in the silicate minerals are the result of Si-O bond vibrations and are easily detectable using thermal infrared remote (TIR) sensing (see Fig. 8).

Samples collected from the base of the monzonite bedrock and recently active washes were subjected to the same linear deconvolution analysis using the four primary end members identified in the dunes.

RESULTS

Petrographic Analysis

The Kelso sand grains were found to be rounded to subrounded with diameters ranging from <150 μm (mafic and opaque minerals) to

400 μm (quartz, feldspar, and lithic fragments), in close agreement with the original work by Sharp (1966). Four primary minerals occur in significant proportions—quartz, plagioclase feldspar, potassium feldspar, and magnetite (Table 1). Amphibole, pyroxene, biotite, calcite, and lithic fragments constitute <5% of the total. In addition, several samples collected from low-lying areas contained appreciable amounts of clay adhered to the other mineral grains. The clay component, analyzed by X-ray diffraction, was identified as primarily montmorillonite.

Samples K1-K6 were taken from the crests and

swales of three adjacent active dunes in the southeast portion of the field. On the basis of field inspection and comparison to the decorrelation stretch image (Fig. 4), these samples should contain a similar distribution of minerals. The point-count data show a standard deviation of 6%–7%, indicating that variability occurs on the scale of the samples and thin section that is not evident in the 17 m/pixel 1985 TIMS image. However, this variability is less than that of the remaining samples (~13%) taken from other areas of the dune field. The results shown in Table 2 indicate that samples K13–K42 have clear mineralogic variations

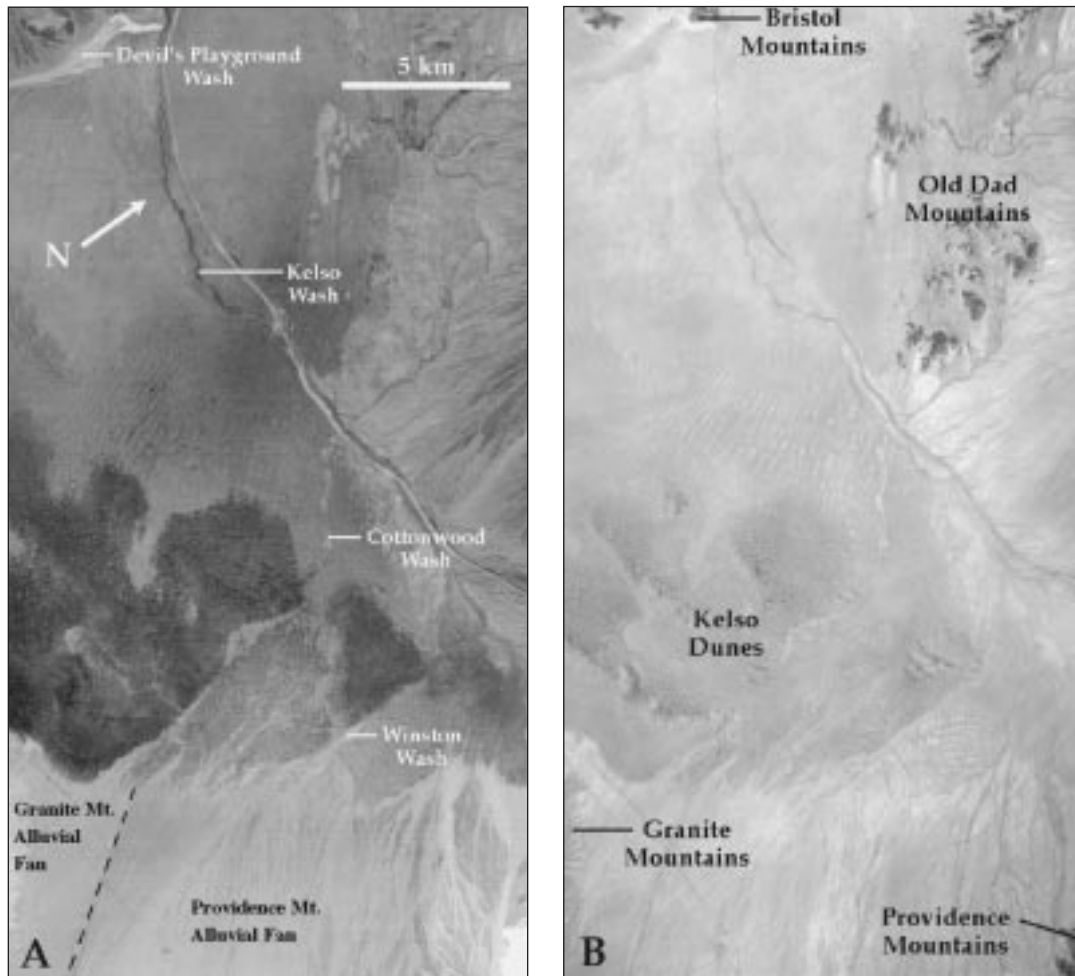


Figure 8. Products of the emissivity-temperature separation of the thermal infrared multispectral scanner (TIMS) data. (A) Band 3 ($9.2\ \mu\text{m}$) emissivity image with darker areas indicating emissivity lows or strong absorptions. The areas of active sand show the largest absorption indicating the presence of quartz and feldspar. In contrast, dolomite in the Providence Mountains and the large amount of magnetite and clay in the washes have the weakest spectral features and appear brightest. (B) Surface brightness temperature image between 41 and $70\ ^\circ\text{C}$. Rock outcrops in the Old Dad, Providence, and Bristol Mountains are cooler and appear darker than the alluvium and sand of the valley. Because of the low topography and time of the overflight, very few thermal shadows are present.

throughout the dune field. These variations appear real based upon (1) the color variations in Figure 4; (2) the differences in the laboratory emission spectra of the 48 sand samples; and (3) the similar results from samples K1–K6 that confirm the repeatability and accuracy of the point-count procedure.

Upon normalizing the point-count data to the four primary minerals, the average dune composition was determined to be 25% potassium feldspar, 29% plagioclase feldspar, 42% quartz, and 4% opaques. A further normalization to remove the opaque minerals results in the proportions of the silicate minerals present in the dunes (Fig. 9A). By combining the values of plagioclase and potassium feldspar, the ternary plot of quartz, feldspar, and opaque shown in Figure 9B reveals a bulk dune composition with a much greater

amount of feldspar than the 10%–30% given by earlier studies (Sharp, 1966; Yeend et al., 1984).

Because samples K1–K6 were taken from the crest and swale of three adjacent dunes, the exact location of each pair could not be distinguished at the TIMS image resolution. Therefore, only the crest samples (K1, K3, and K5) are used in all subsequent comparisons, reducing the number of petrographically analyzed samples from 13 to 10. Applying the retrieval algorithm using the four library-derived end members to the spectra of these 10 remaining samples produced the modeled mineral percentages shown in Table 3. These results, when compared to the petrographic analysis, reveal a model difference ranging from 0.2% to 10.4%; the overall average is 3.11%. The model fit shown by the RMS error was 6.54×10^{-3} , indicating that the difference between the measured

and model spectra was $<1\%$. Figure 10 shows an example of one such model fit for the spectrum of sample K13. The largest residual errors occur over the strong absorption bands, approaching 2% at several wavelength regions. The small magnitude of these errors is notable, considering that no attempt was made to represent the exact feldspar compositions of the sands with the library end-member spectra. Oligoclase and microcline were chosen simply as average representations of typical feldspar mineralogy in the area. The larger residuals at $1050\ \text{cm}^{-1}$ ($9.52\ \mu\text{m}$), $1000\ \text{cm}^{-1}$ ($10.0\ \mu\text{m}$), and $600\ \text{cm}^{-1}$ ($16.7\ \mu\text{m}$) are due to the vibrational absorptions of feldspar (Nash and Salisbury, 1991) and therefore indicate a probable unmodeled feldspar composition. A study by Reheis and Kihl (1995) of regional dust deposition in the area not only in-

TABLE 2. POINT COUNT RESULTS FOR KELSO SAMPLES (K1-K42)

Sample number	Plagioclase (%)	Microcline (%)	Quartz (%)	Opaque (%)	Other (%)
Individual results					
K1c	17.00	32.00	42.50	3.00	5.50
K2s	27.00	29.00	40.50	1.00	2.50
K3c	32.50	24.50	40.00	1.00	2.00
K4s	28.00	30.50	38.50	0.50	2.50
K5c	33.50	28.50	35.50	0.50	2.00
K6s	33.50	29.00	34.50	1.00	2.00
K13c	19.50	26.50	51.00	1.50	1.50
K17c	38.50	19.50	36.50	2.00	3.50
K22s	29.30	18.00	41.70	3.00	8.00
K23c	30.50	18.00	45.50	0.50	5.50
K24c	29.70	9.30	29.00	23.00	8.90
K40c	25.00	20.50	36.50	13.00	5.00
K42c	18.50	24.00	53.50	0.50	3.50
Averaged results					
Average (all)	27.88	23.79	40.40	3.88	4.03
Average (K1-K6)	28.58	28.92	38.58	1.17	2.75
Standard deviation	6.70	6.42	6.47	2.39	6.65
Minimum	29.00	18.50	9.30	1.50	0.50
Maximum	53.50	38.50	30.50	8.90	23.00

indicates a chemistry that is more abundant in feldspar than quartz (similar to results presented here), but also that the feldspar composition is more calcium rich than the oligoclase used here.

TIMS Image Analysis

The blind end-member investigation into the ability of the model to choose the correct end-member suite from a subset of the entire library proved highly successful, although computationally intensive. For example, a set of the most likely 15 minerals at Kelso produced 375 unique combinations of less than four end members. From this set, the algorithm chose the four presented here as the most likely combination. This choice was based purely on the lowest overall RMS error for the quartz-microcline-oligoclase-clay + magnetite suite. Other minerals were found in higher abundances in the image, including cal-

cite in the Providence Mountain carbonate outcrop and alluvial fan, and hornblende in many of the same areas identified as clay + magnetite. Yeend et al. (1984) noted the presence of hornblende and mentioned the weathering of metasedimentary rocks in the Granite Mountains as the source for it and the magnetite. This seems logical on the basis of the petrographic and spectral deconvolution information presented here.

After the model was used to deconvolve the 1995 TIMS data, the predicted mineral percentages and RMS error were extracted from the images at each sample site (Fig. 11). Sample numbers represent a south-north traverse into the dune field (closer to the center of the TIMS image). Due to the degradation to six-point TIMS spectra (see Discussion), there was a slight reduction in the accuracy of the model fit compared to the results of the laboratory deconvolution (Table 3). The average model difference and

RMS error increased to 5.3% and 8.90×10^{-3} , respectively. Summing the model difference over the number of samples for every end member produced an average error for that mineral. Comparing this average for the TIMS results to those of the laboratory deconvolution indicates virtually no change for the clay + magnetite (2%) and oligoclase (3%) end members (Fig. 11, A and C). However, the errors for microcline and quartz increased 6.3% and 3.4%, respectively (Fig. 11, B and D). Similarly, the RMS error (Fig. 11E) shows values that are nearly twice as large at the beginning of the sampling (image edge) as at the end (image center). The increase in model RMS error with distance from the image edge is due to the incomplete atmospheric correction.

The clay + magnetite end member is virtually nonexistent within the active dunes (Fig. 12A), which agrees with the low overall average of 4.2% derived from the point counts. It appears that the model is insensitive to abundances lower than 5% for this generally featureless spectral end member. Samples K1-K23 have from 0.5% to 3.3% opaques, and yet the model, applied to the TIMS data, predicts no clay + magnetite (Fig. 11A). Stronger concentrations of this end member occur on the alluvial fans extending from the Granite Mountains to the south and Providence Mountains to the east, and on the stabilized dunes and sand sheets to the north. Visible concentrations within the active field occur in low-lying vegetated areas between the three large active linear ridges. These act as traps for eolian fines that are spectrally similar to the clay + magnetite end member.

The microcline end member (Fig. 12B) is generally overpredicted by the model by nearly 9%. Despite this higher concentration, which is assumed uniform throughout the image, the microcline is clearly concentrated in the active dune

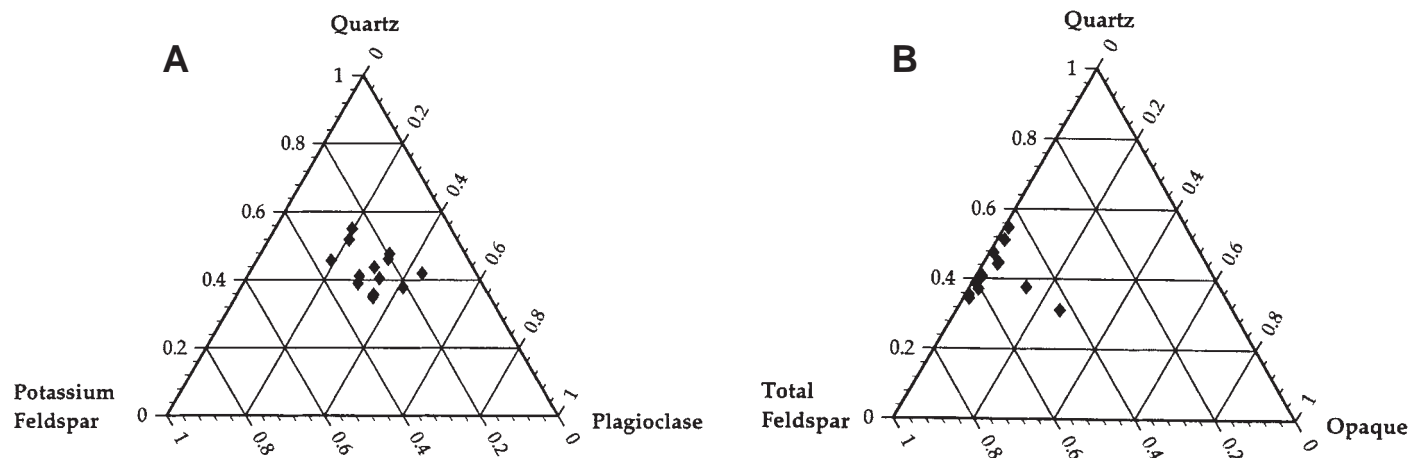


Figure 9. Ternary plots of the average Kelso dune sands derived from point counts of the 13 thin-section samples. (A) Normalized to the silicate mineralogy. (B) The four primary minerals shown by summation of the plagioclase and potassium feldspars.

sand and on the alluvial fan to the east. Samples collected here, although not verified using petrography, contained model-identified microcline in decreasing percentages (Table 4) from 67% (coarse grus) to 57% (Winston wash). At the crest of a series of active dunes directly across from the wash, the microcline percentage dropped to 45%. This value is still higher than the derived average for the original samples, but not out of the range found in other parts of the dune field. There is a noticeable decline in the mineral percentage within the stabilized areas directly surrounding the field and between the main ridges. These areas contain more eolian fines and vegetation and map as mostly clay + magnetite with lesser amounts of oligoclase.

The oligoclase end member (Fig. 12C) is most strongly concentrated on the alluvial fan originating from the Granite Mountains, in less active zones surrounding the main field, and to the north within the dunes. The pattern of mineral distribution also shows higher concentrations in the low-lying areas on the lee sides of the large linear ridges. It is possible that the high concentrations on the alluvial fans may be overestimated due to the atmospheric effects. However, there appears

to be a coherent distribution pattern throughout the image and not simply higher amounts of the mineral solely on the edges. There is a large region to the northwest of the dunes that contains little oligoclase end member. This region, concentrated in quartz relative to oligoclase, is closest to sands transported through the Devils Playground.

Quartz, the single-most abundant mineral from the point-count data, is much more evenly distributed throughout the scene except for east-

northeast of the dunes (Fig. 12D). This important boundary in the dune field known as Cottonwood wash separates active from highly inactive dune surfaces (Paisley et al., 1991). The model-predicted quartz content is much less in these inactive regions, yet still very distinguishable from the alluvial fan surface to the east. In this way, the quartz end-member image serves as an indicator of dune activity levels, analogous to the use of albedo in the VNIR by Paisley et al. (1991).

TABLE 3. RETRIEVAL ALGORITHM RESULTS DERIVED FROM LABORATORY DATA

Sample number	Oligoclase (%)	Microcline (%)	Quartz (%)	Clay + Magnetite (%)	Residual (sample) (%)	RMS* error
K1c	19.97	32.23	48.17	0.00	2.50	7.26E-03
K3c	35.44	23.21	39.26	2.11	1.68	7.12E-03
K5c	36.73	25.37	37.90	0.00	2.11	6.54E-03
K13c	29.39	25.50	44.01	1.72	4.74	6.32E-03
K17c	36.30	21.57	37.65	5.23	2.07	6.40E-03
K22s	32.70	21.19	43.15	3.71	1.28	6.67E-03
K23c	34.43	23.12	37.74	5.24	5.34	5.89E-03
K24c	37.48	15.25	28.44	19.39	4.80	6.32E-03
K40c	31.09	21.21	38.20	10.05	2.25	6.19E-03
K42c	25.60	25.85	46.94	1.99	4.35	6.66E-03
Residual (end member)	3.90	2.20	3.91	2.43	3.11	N.A.

*RMS—root-mean-squared. N.A.—not available.

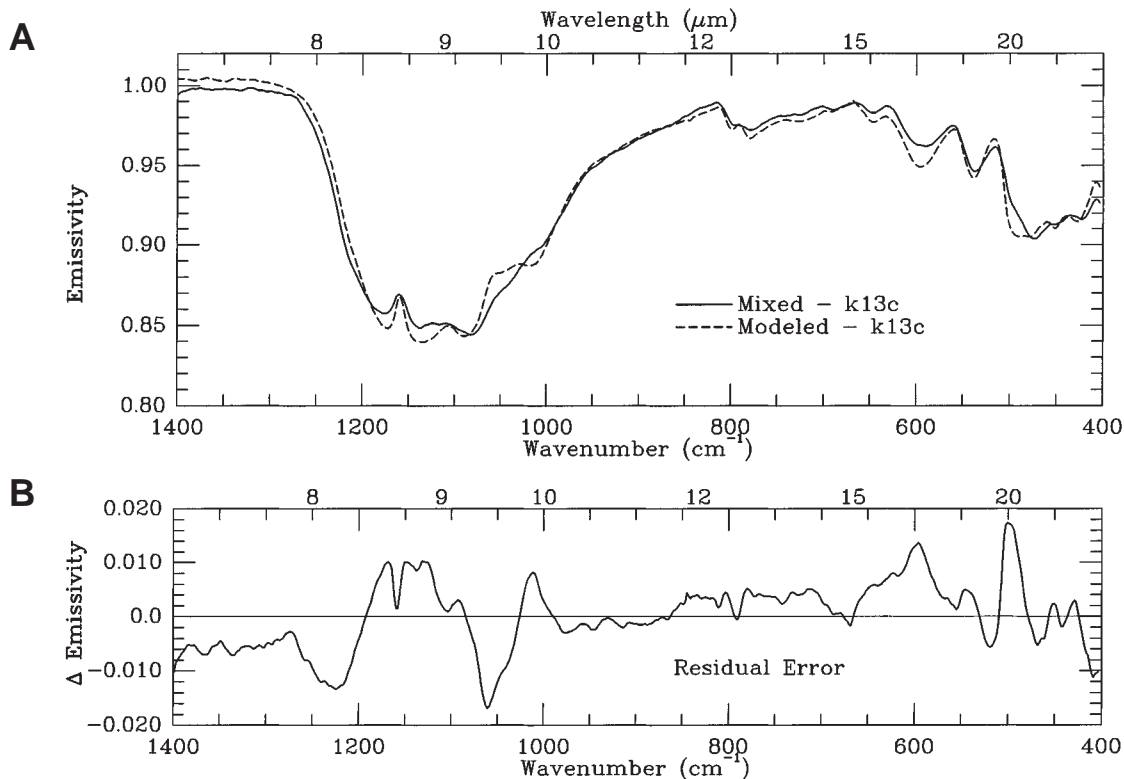


Figure 10. Retrieval model results for the laboratory spectrum of sample K13. (A) Fit using the library end members in Figure 7. (B) The residual error (measured-modeled) shows the regions of poor fit over the large absorption bands. These errors approach 2% at 1050 cm^{-1} (9.5 μm) and 500 cm^{-1} (20 μm) and are due to unmodeled feldspar features. The average root-mean-squared error for this deconvolution iteration was 0.63%, indicating a good fit.

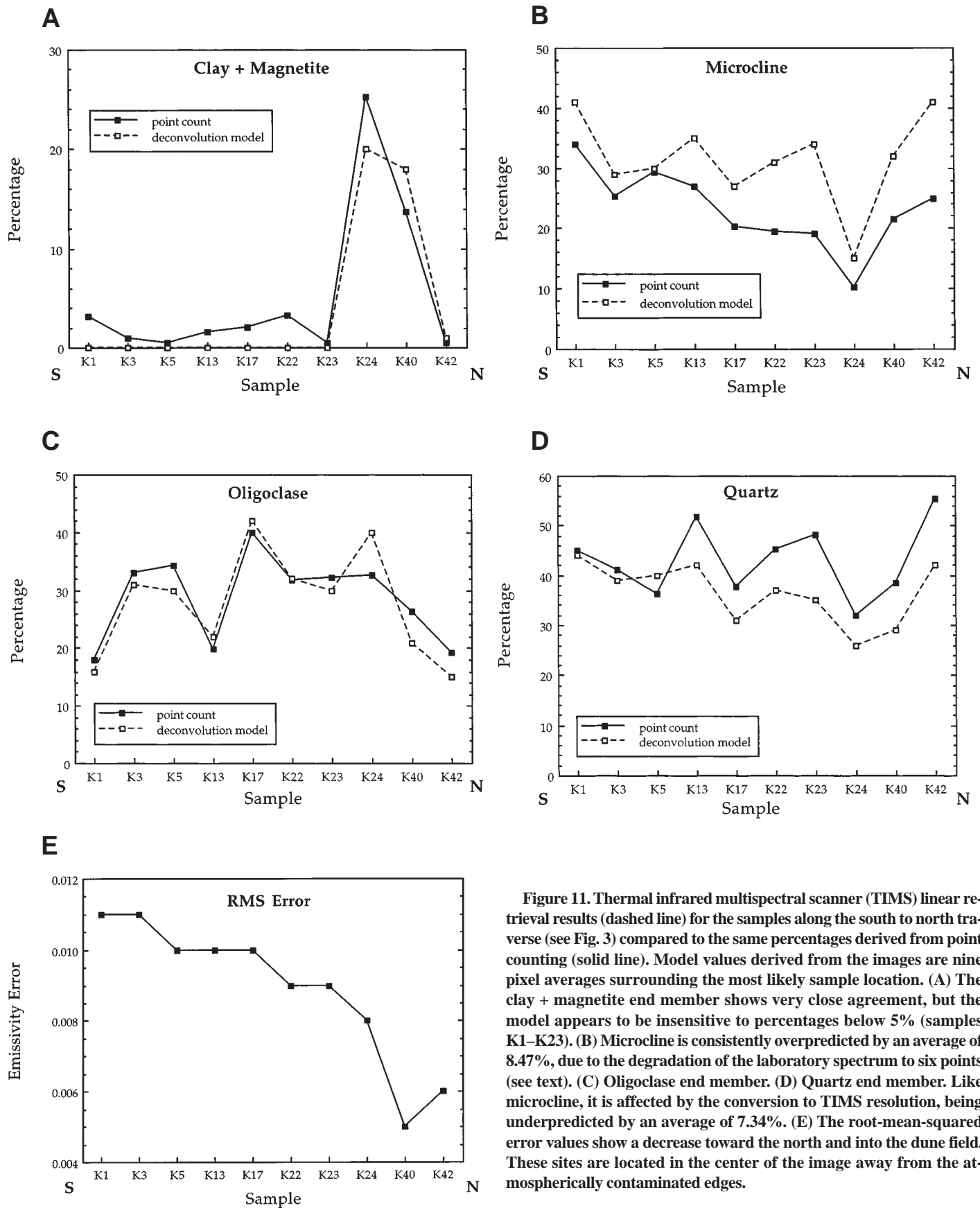


Figure 11. Thermal infrared multispectral scanner (TIMS) linear retrieval results (dashed line) for the samples along the south to north traverse (see Fig. 3) compared to the same percentages derived from point counting (solid line). Model values derived from the images are nine pixel averages surrounding the most likely sample location. (A) The clay + magnetite end member shows very close agreement, but the model appears to be insensitive to percentages below 5% (samples K1–K23). (B) Microcline is consistently overpredicted by an average of 8.47%, due to the degradation of the laboratory spectrum to six points (see text). (C) Oligoclase end member. (D) Quartz end member. Like microcline, it is affected by the conversion to TIMS resolution, being underpredicted by an average of 7.34%. (E) The root-mean-squared error values show a decrease toward the north and into the dune field. These sites are located in the center of the image away from the atmospherically contaminated edges.

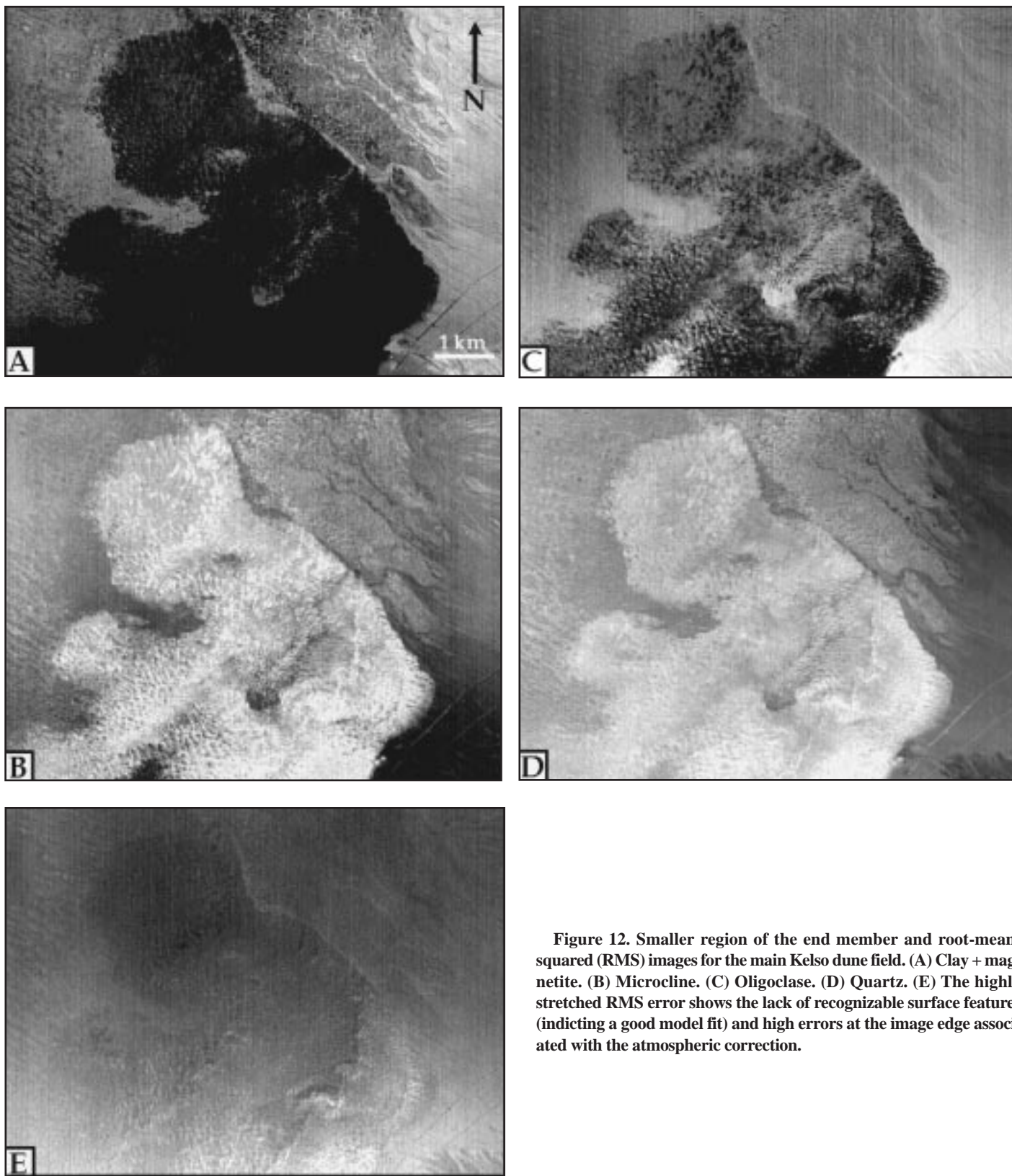


Figure 12. Smaller region of the end member and root-mean-squared (RMS) images for the main Kelso dune field. (A) Clay + magnetite. (B) Microcline. (C) Oligoclase. (D) Quartz. (E) The highly stretched RMS error shows the lack of recognizable surface features (indicating a good model fit) and high errors at the image edge associated with the atmospheric correction.

TABLE 4. RETRIEVAL ALGORITHM RESULTS FOR PROVIDENCE MOUNTAIN FAN

Sample number	Oligoclase (%)	Microcline (%)	Quartz (%)	Clay + Magnetite (%)	RMS* error
Granite (coarse)	0.14	67.50	32.37	0.00	1.92E-02
Granite (fine)	0.13	59.46	40.34	0.07	8.08E-03
Winston Wash	0.11	57.31	31.45	11.12	7.88E-03
Dune crest	0.09	45.20	54.71	0.00	1.71E-02

*RMS—root-mean-squared.

The RMS error shows an increase toward the image edge (Fig. 12E) as a result of the atmospheric contamination still present after the MODTRAN correction. The image, highly stretched from 0% to 0.5% (5 DN), shows very little structure due to topographic features over the regions of good model fit. This and the very small values of the RMS indicate that most of the retrieval errors are confined to atmospheric and instrument noise, and denote a high level of confidence for the model fit (Gillespie et al., 1990). The overall RMS error is ~0.2% lower within the active region of the dunes. This is to be expected because the active dunes commonly contain only the four modeled end members, whereas the surrounding stabilized dunes are spectrally more complex due to the presence of vegetation, lithic material, and trapped eolian fines.

DISCUSSION

Petrographic Analysis

The analysis presented here represents the most detailed petrologic study of the Kelso sands to date. Significant to the question of the maturity and sources of sediment for Kelso was the finding that the dunes contain far less quartz than previous workers have estimated. The roughly equal amounts of potassium feldspar and plagioclase feldspar, together summing to greater than the percentage of quartz, more closely reflect the local geology of the region. This finding may indicate a dune field that has been incorporating local source material in greater quantities over longer periods than previously reported. Furthermore, no study to date has attempted to perform an accurate separation of potassium feldspar from plagioclase feldspar. The use of microcline as a spectral end member in the linear retrieval analysis reveals a potential local source from the Providence Mountains to the east.

The original study by Sharp (1966) gave an overall composition of quartz, feldspar, opaques, and lithic fragments as 70%–80%, 10%–30%, 5%–10%, and 3%–10%, respectively. Subsequent investigations have referenced these values (Yeend et al., 1984; Lancaster, 1993, 1994). Paisley et al. (1991) reported an extreme 90% quartz and 10%

other (mainly opaques) based on point-count information, but no mention was made about the quality, quantity, or methodology of the analysis. It seems clear that no attempt was made to distinguish feldspar from quartz, and their results should be questioned. The high quartz content mentioned in these earlier studies assumes a dune field with a past sediment source originating at the Mojave River Wash 50 km to the west. With such a large transportation distance and amount of chemical and mechanical weathering, the winnowing of other minerals would result in a concentration of quartz and to a lesser degree plagioclase. However, based on this work, that appears not to have happened to such a degree in the Kelso Dunes.

Spectral Analysis

Library spectra used in this study can accurately deconvolve and model naturally occurring eolian sediment to within the level of precision of the laboratory spectrometer (Ruff et al., 1997; Ramsey and Christensen, 1998). In general, the oligoclase and clay + magnetite end members show excellent agreement with the percentages derived from the point counts. However, quartz is commonly underpredicted and microcline is overpredicted in all the samples. There are two possible explanations for this discrepancy. (1) The least likely possibility is that the error is attributed to inaccurately locating the original sample collection site on the image, and/or the mineralogy of the site has changed in five years. Because of the good agreement of the other two end members and the averaging of nine pixels where extracting the values, it is doubtful that the sample sites were not correctly pinpointed. Furthermore, it is unclear what process could differentially concentrate microcline, decrease quartz, and yet leave the other two minerals unchanged over five years. Therefore, surface change over the course of several years is implausible, especially considering the documented lack of dune variability in the 15 yr study of Sharp (1966). (2) A more likely cause of the error is the spectral degradation that occurs where translating laboratory data to TIMS spectra. This effect is most pronounced in mineral spectra with broad and/or very small-scale absorption bands, which tend to be compressed and reduced in contrast where convolved to the six-

point TIMS resolution. Both quartz and microcline have the strongest absorption bands of the four end members and thus are affected the most upon degradation.

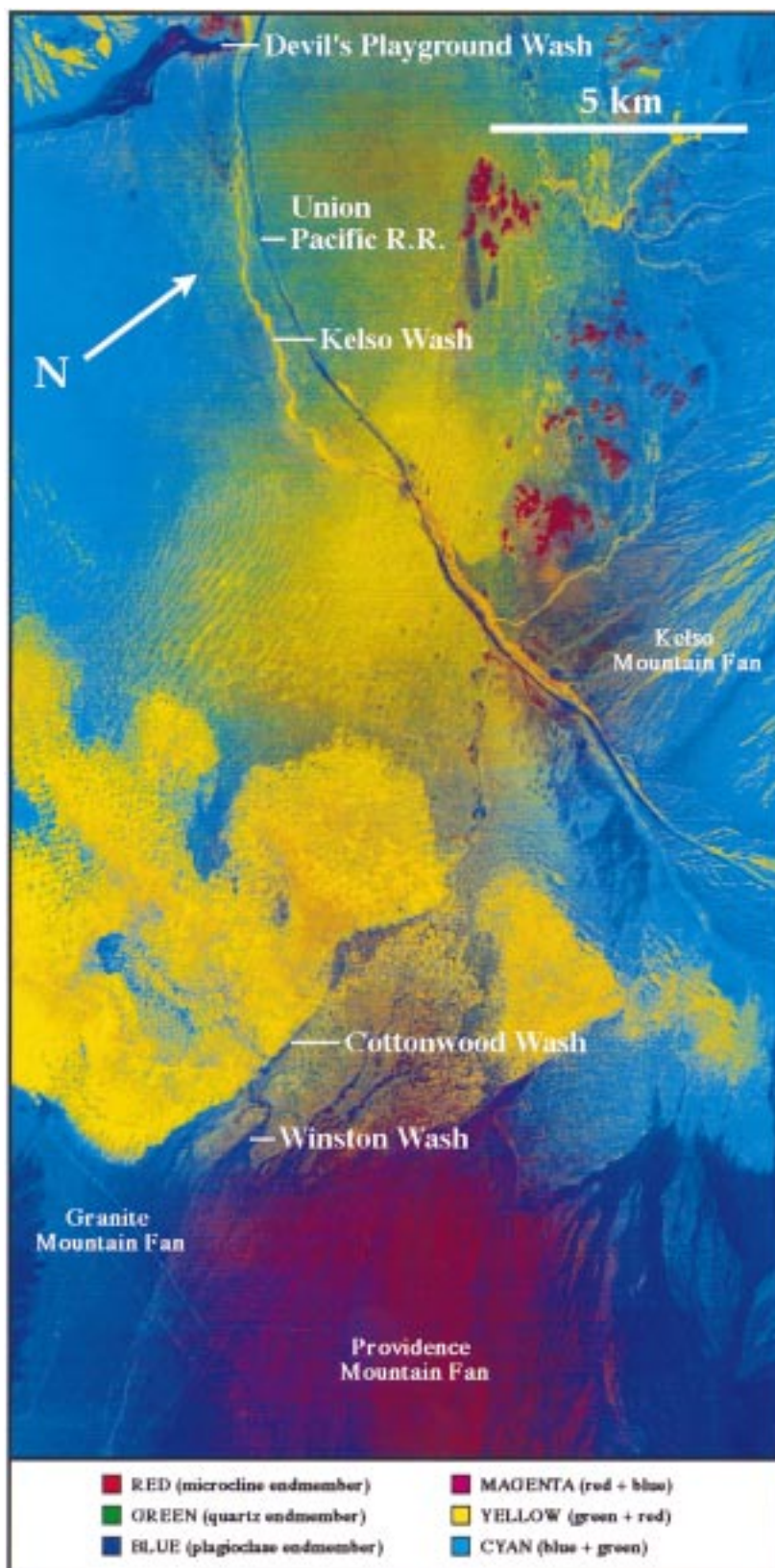
Local Microcline Source

The microcline distribution within the dunes is slightly higher to the south and concentrated more along the crests of the linear ridges. The point-count data (Fig. 11B) confirm this increase, showing an ~10% higher average for microcline in samples K1–K13 than in the remaining thin sections. This concentration of microcline could be due to the input from a proximal source at the south end of the field, or a preferential eolian sorting based on the slight density difference between the end-member minerals. The lower density of microcline (2.5–2.6) is similar to that of quartz (2.65), which also shows a slight, but not statistically significant, concentration to the south (Fig. 12D). Oligoclase varies in density (2.67–2.76) with increasing calcium content and appears to be slightly concentrated to the north of the active dune field (Fig. 12C). However, such a minor difference in density between the silicate end-member minerals is highly unlikely to result in preferential grain sorting. The more likely scenario is that microcline, weathering out of the monzonite alluvium present on the Providence Mountain fans, is incorporated into the dunes. This material would be transported into the central part of the field by fluvial activity and the intermittent orographic winds from the east. The prevalent winds from the northwest could then transport the microcline by way of saltation, thereby causing the increase in the southern portion of the dune field.

This is more clearly visible in the silicate end-member color composite (Fig. 13). Images displayed in this manner permit regions of overlap and mixing within two or more of the gray-scale images to be easily distinguished. The dune field appears dominantly yellow, indicating nearly equal amounts of quartz and microcline. The yellow is brightest toward the southern end of the field, highlighting a stronger concentration of each mineral. There also appears to be a slightly higher concentration of quartz and oligoclase in the western portion of the dunes and in the low areas between the ridges (more green and cyan). The quartz being introduced from the west and the oligoclase dominating the Granite Mountain fans are both farther from the microcline source to the east. The lower amount of microcline in this region would have the same effect on the color composite as a higher concentration of quartz and oligoclase.

An increased level of microcline along the crest and lee side of the northernmost large linear

Figure 13. Thermal infrared multispectral scanner (TIMS) three-color composite for the entire scene, showing microcline in red, quartz in green, and oligoclase in blue. Yellow indicates a nearly equal abundance of quartz and microcline, whereas cyan is quartz + oligoclase. Microcline, entering from the eastern fan of the Providence Mountains, appears to have been transported over the Cottonwood and Winston Washes and incorporated into the active dunes (orange). Oligoclase is being derived from the northern and southern alluvial fans, and in addition occurs to a lesser extent along the Mojave River Wash–Kelso Dune transport path. The slight greenish coloration within the transport path indicates that quartz is the dominant mineral and is transported from the west. Quartz and microcline also appear to be being remobilized out of the Kelso Wash near the point where the railroad tracks and the wash diverge. It is likely that these sands are being deposited into the dunes by the prevailing easterly winds.



ridge is indicated by the orange swath extending east to west (Fig. 13). This zone indicates the potential microcline input location into the dunes from the fan source to the east. There is a more subtle zone of red that bisects the inactive dunes to the east of Cottonwood Wash, which appears to delineate the transport path from the alluvial fan to the dunes. This mixing pattern is not visible by means of any other processing tool used on the TIMS data. More important, this slight mineralogical variation can not be identified with other remote-sensing instruments operating in different wavelength regions. These image results are confirmed by the samples collected along this path.

Expanding outward from the area immediately surrounding the dunes, many of the surrounding input sources become visible. The alluvial fans that surround the valley (sides of the image) map as shades of blue and cyan, indicating a predominantly oligoclase mineralogy with varying amounts of quartz. These fans originate from the metasedimentary rocks of the Granite Mountains to the south and the monzonite and Proterozoic crystalline rocks of the Kelso Mountains to the north (Jennings, 1961). To the northeast of the active field the dunes also show as cyan and blue, indicating the high oligoclase content in this area (Lancaster, 1993).

The two major washes in the scene appear to be responsible for transporting material to the northwest of the dunes. This material can then be remobilized and transported back to the Kelso sediment sink (Yeend et al., 1984). The Kelso Wash extends west and drains the mountains to the northeast (Jennings, 1961) of the dunes and is paralleled by the Union Pacific railroad tracks. It shows as blue to yellow to the north of the dunes and increases in red as potassium feldspar weathering from nearby granite inselbergs is entrained into its bed. These outcrops are coated with desert varnish and their spectral signature is strongly affected by this coating (Christensen and Harrison, 1993). The magenta region to the east of these outcrops appears to be a mixing of the oligoclase from the alluvial fans and the weathering of the varnished granite. In the region of the intersection of the wash and the railroad tracks, the quartz and microcline grains are apparently mobilized by the wind and deposited on the sand sheet to the west of the Kelso Dunes. At the confluence of the Kelso wash and the Devils Playground Wash, the dark blue to black color mapped by the algorithm indicates mostly clay + magnetite and oligoclase. The wash drains the amphibole-rich metasedimentary rocks of the Granite and Bristol Mountains and seems to be a strong source for the mafic and opaque minerals present in the Kelso sands (Yeend et al., 1984; Lancaster, 1993), as opposed to the Mojave River source (Sharp, 1966).

CONCLUSIONS

TIMS data originally provided the impetus for the sample collection and initiated the petrographic analysis of the sand mineralogy at the Kelso Dunes. However, it was not until the development and application of the linear retrieval model that examination of specific mineral distributions became possible. This study represents a rigorous attempt to quantify and validate the linear mixing assumption of thermal emission spectra for an active geologic surface. It also is one of the most detailed petrologic studies of the Kelso Dunes sand mineralogy. In combination, they provide an excellent validation for the linear retrieval algorithm using library mineral spectra in conjunction with remotely acquired data. The results show that there are clear mineralogical variations throughout the dunes and that the field on average contains 40%–50% quartz, significantly less than previous work had stated. The general agreement between the petrographic and spectral analyses is noteworthy, considering the 5 yr difference between image and sample collection, as well as the scale difference between image and laboratory samples.

Mineral end-member images show very high concentrations of microcline within the dunes as well as on alluvial surfaces extending from the immediate mountain ranges. This relation, which may indicate that a percentage of the sand in the dune field is locally derived, has never been noted in the past. In a similar way, the magnetite and other mafic minerals seem to be the direct result of weathering of local amphibole-rich metasedimentary rocks in the Granite Mountains (Yeend et al., 1984). By contrast, whereas a certain percentage of the quartz within the dunes is also likely derived locally, there is no evidence of a direct near-field source. On the basis of higher concentrations to the northwest, it appears that the dominant percentage of this mineral may originate from alluvial material deposited at the Mojave River Wash to the west.

Detailed geomorphic and mineralogical studies of eolian deposits and land forms, using thermal infrared remote sensing, show that transport of sand in the Kelso eolian system initiates from several sources. Lancaster (1994) indicated that formation of new eolian deposits in this area has been strongly influenced by sediment availability, which is in turn related to regional climatic changes (Wells and McFadden, 1987). These changes of a lower amplitude appear to control dune activity on shorter time scales and may be responsible for the activation of new sediment sources and the decline of others.

Investigations such as this one will greatly benefit similar data analyses and future applications. With the launch of the Advanced Space-

borne Thermal Emission and Reflectance Radiometer (ASTER) instrument (Kahle et al., 1991) in July 1999, multispectral global TIR data will become available for the first time. Such data can provide the geologist with a synoptic look at an entire eolian system over different time scales, allowing an inference of past activity and the monitoring of current climate changes. Drought-prone areas on the metastable margins of these transport pathways and sand seas are easily susceptible to dune encroachment and possible desertification with environmental change. Human activity in these regions will benefit from repetitive monitoring programs using ASTER data in conjunction with analysis techniques such as linear deconvolution.

ACKNOWLEDGMENTS

We thank Ken Edgett for numerous discussions on sand transport and his assistance in the field, as well as the entire crew of the NASA C130 aircraft program for their extra effort and dedication in acquiring both data sets. The quality of this manuscript was greatly improved thanks to helpful reviews by Larry Rowan, Marith Reheis, and an anonymous reader. Research funding for this study has been provided by NASA through the Planetary Geology and Geophysics Program as well as the Mission to Planet Earth, ASTER science project.

REFERENCES CITED

- Barbera, P. W., 1989, Geology of the Kelso-Baker region, Mojave Desert, California using thermal infrared multispectral scanner data [Master's thesis]: Tempe, Arizona State University, 198 p.
- Beckerman, G. M., Robinson, J. P., and Anderson, J. L., 1982, The Teutonia Batholith: A large intrusive complex of Jurassic and Cretaceous age in the eastern Mojave Desert, California, in Frost, E. G., and Martin, D. L., eds., Mesozoic-Cenozoic tectonic evolution of the Colorado River region, California, Arizona, and Nevada (Anderson-Hamilton Volume): San Diego, Cordilleran Publishers, p. 205–220.
- Berke, A., Bernstein, L. S., and Robertson, D. C., 1989, MODTRAN: A moderate-resolution for LOWTRAN 7: U.S. Air Force System Command, Geophysical Laboratory Report GL-TR-89-0122, 137 p.
- Bishop, C. C., 1963, Geologic map of California, Needles sheet: Department of Natural Resources, California Division of Mines and Geology, scale: 1:250 000, 1 sheet.
- Bissell, H. J., 1974, Tectonic control of late Paleozoic and early Mesozoic sedimentation near the hinge line of the Cordilleran miogeosynclinal belt, in Dickinson, W. R., ed., Tectonics and sedimentation: Society of Economic Paleontologists and Mineralogists Special Publication 22, p. 83–97.
- Blount, G., Smith, M. O., Adams, J. B., Greeley, R., and Christensen, P. R., 1990, Regional aeolian dynamics and sand mixing in the Gran Desierto: Evidence from Landsat Thematic Mapper images: Journal of Geophysical Research, v. 95, p. 15463–15482.
- Breed, C. S., and Grow, T., 1979, Morphology and distribution of dunes in sand seas observed by remote sensing, in McKee, E. D., ed., A study of global sand seas: U.S. Geological Survey Professional Paper 1052, p. 253–301.
- Breed, C. S., McCauley, J. F., Breed, W. J., McCauley, C. K., and Cotera, A. S., Jr., 1984, Eolian (wind formed) land-

- scapes, in Smiley, T. L., Nations, J. D., Pewe, T. L., and Schafer, J. P., eds., *Landscapes of Arizona: The geological story*. New York, University Press of America, 505 p.
- Cadle, R. D., 1955, Particle size determination: New York, Interscience Publishers, p. 57–58.
- Christensen, P. R., and Harrison, S. T., 1993, Thermal-infrared emission spectroscopy of natural surfaces: Application to desert varnish coatings on rocks: *Journal of Geophysical Research*, v. 98, p. 19819–19834.
- Clark, R. N., 1983, Spectral properties of mixtures of montmorillonite and dark carbon grains: Implications for remote sensing minerals containing chemically and physically adsorbed water: *Journal of Geophysical Research*, v. 88, p. 10635–10644.
- Clarke, M. L., 1994, Infra-red stimulated luminescence ages from aeolian sand and alluvial fan deposits from the eastern Mojave Desert, California: *Quaternary Science Reviews*, v. 13, p. 533–538.
- Edgett, K. S., and Anderson, D. L., 1995, For geologic investigations with airborne thermal infrared multispectral images: Transfer of calibration from laboratory spectrometer to TIMS as alternative for removing atmospheric effects, in Realmuto, V. J., ed., *Summaries Fifth Annual Airborne Earth Science Workshop*, Volume 2: Pasadena, California, Jet Propulsion Laboratory Publication 95–1, p. 9–12.
- Edgett, K. S., Ramsey, M. S., and Christensen, P. R., 1995, Aeolian erosion, transport, and deposition of volcanoclastic sands among the Shifting Sand Dunes, Christmas Lake, Oregon: TIMS image analysis, in Realmuto, V. J., ed., *Summaries, Fifth Annual Airborne Earth Science Workshop*, Volume 2: Pasadena, California, Jet Propulsion Laboratory Publication 95–1, p. 13–16.
- Edwards, S. R., 1993, Luminescence dating of sand from the Kelso Dunes, California, in Pye, K., ed., *Dynamics and environmental context of aeolian sedimentary systems*: Geological Society [London] Special Publication 72, p. 59–68.
- Gillespie, A. R., 1992, Spectral mixture analysis of multispectral thermal infrared images: *Remote Sensing of the Environment*, v. 42, p. 137–145.
- Gillespie, A. R., Kahle, A. B., and Walker, R. E., 1986, Color enhancement of highly correlated images: I. Decorrelation and HSI contrast stretches: *Remote Sensing of the Environment*, v. 20, p. 209–235.
- Gillespie, A. R., Smith, M. O., Adams, J. B., Willis, S. C., Fischer, A. F., III, and Sabol, D. E., 1990, Interpretation of residual images: Spectral mixture analysis of AVIRIS images, Owens Valley, California, in Green, R. A., ed., *Proceedings, Second Annual Airborne Earth Science Workshop*, Volume 1: Jet Propulsion Laboratory Publication 90–54, p. 1–28.
- Hapke, B., 1981, Bidirectional reflectance spectroscopy, 1. Theory: *Journal of Geophysical Research*, v. 86, p. 3039–3054.
- Jennings, C. W., 1961, Geologic map of California, Kingman Sheet: Department of Natural Resources, California Division of Mines and Geology, scale: 1:250 000, 1 sheet.
- Johnson, P. E., Smith, M. O., Taylor-George, S., and Adams, J. B., 1983, A semiempirical method for analysis of the reflectance spectra of binary mineral mixtures: *Journal of Geophysical Research*, v. 88, p. 3557–3561.
- Johnson, P. E., Smith, M. O., and Adams, J. B., 1992, Simple algorithms for remote determination of mineral abundances and particle sizes from reflectance spectra: *Journal of Geophysical Research*, v. 97, p. 2649–2657.
- Jones, M. P., 1987, Applied mineralogy: A quantitative approach: Norwell, Massachusetts, Graham and Trotman, p. 74–75.
- Kahle, A. B., and Goetz, A. F. H., 1983, Mineralogic information from a new airborne thermal infrared multispectral scanner: *Science*, v. 222, p. 24–27.
- Kahle, A. B., Palluconi, F. D., Hook, S. J., Realmuto, V. J., and Bothwell, G., 1991, The advanced spaceborne thermal emission and reflectance radiometer (ASTER): *International Journal of Imaging System Technology*, v. 3, p. 144–156.
- Lancaster, N., 1990, Dune morphology and chronology, Kelso Dunes, Mojave Desert, California: Geological Society of America Abstracts with Programs, v. 22, no. 7, p. A86.
- Lancaster, N., 1993, Development of the Kelso Dunes, Mojave Desert, California: *National Geographic Research and Exploration*, v. 9, p. 444–459.
- Lancaster, N., 1994, Controls on aeolian activity: Some new perspectives from the Kelso Dunes, Mojave Desert, California: *Journal of Arid Environments*, v. 27, p. 113–125.
- Leonidov, V. A., 1989, Remote sensing of reclaimed lands and adjacent territories in the fight against desertification: *Problems of Desert Development*, v. 3, p. 46–59.
- McDonald, E., and McFadden, L. D., 1994, Quaternary stratigraphy of the Providence Mountains piedmont and preliminary age estimates and regional stratigraphic relations of Quaternary deposits in the eastern Mojave Desert, California, in McGill, S. F., and Ross, T. M., eds., *Geological investigations of an active margin* (Geological Society of America Cordilleran Section, 27th annual meeting guidebook): San Bernardino, California, p. 205–210.
- Muhs, D. R., Bush, C. A., Cowherd, S. D., and Mahan, S., 1995, Source of sand for the Algodones Dunes, in Tchakerian, V. P., ed., *Desert aeolian processes*: New York, Chapman and Hall, p. 37–74.
- Mustard, J. F., and Pieters, C. M., 1989, Photometric phase functions of common geologic minerals and applications to quantitative analysis of mineral mixture reflectance spectra: *Journal of Geophysical Research*, v. 94, p. 13619–13634.
- Nash, D. B., and Salisbury, J. W., 1991, Infrared reflectance spectra (2.2–15 μm) of plagioclase feldspars: *Geophysical Research Letters*, v. 18, p. 1151–1154.
- Otterman, J., 1981, Satellite and field studies of man's impact on the surface in arid regions: *Tellus*, v. 33, p. 68–77.
- Paisley, E. C. I., Lancaster, N., Gaddis, L. R., and Greeley, R., 1991, Discrimination of active and inactive sand from remote sensing: Kelso Dunes, Mojave Desert, California: *Remote Sensing of the Environment*, v. 37, p. 153–166.
- Palluconi, F. D., and Meeks, G. R., 1985, Thermal infrared multispectral scanner (TIMS): An investigators guide to TIMS data: Pasadena, California, Jet Propulsion Laboratory Publication 85–32, 14 p.
- Ramsey, M. S., 1996, Object detection utilizing a linear retrieval algorithm for thermal infrared imagery, in *Proceedings, Second International Airborne Remote Sensing Conference*, Volume II: Ann Arbor, Michigan, Environmental Research Institute of Michigan, p. 559–569.
- Ramsey, M. S., and Christensen, P. R., 1997, Monitoring potential desertification via airborne TIR data: Sediment transport in the Mojave Desert, California, in *Proceedings, The First JPL Workshop on Remote Sensing of Land Surface Emissivity*, May 1997: Pasadena, California, Jet Propulsion Laboratory Publication.
- Ramsey, M. S., and Christensen, P. R., 1998, Mineral abundance determination: Quantitative deconvolution of thermal emission spectra: *Journal of Geophysical Research*, v. 103, p. 577–596.
- Ramsey, M. S., Howard, D. A., Christensen, P. R., and Lancaster, N., 1993, Mineralogic variability of the Kelso Dunes, Mojave Desert, California derived from thermal infrared multispectral scanner (TIMS) data, in Realmuto, V. J., ed., *Summaries, Fourth Annual Airborne Earth Science Workshop*, Volume 2: Pasadena, California, Jet Propulsion Laboratory Publication 93–26, p. 9–12.
- Ramsey, M. S., Howard, D. A., Christensen, P. R., and Lancaster, N., 1994, Sand sources and mineralogic variability within the Kelso dune field, Mojave Desert, California: Analysis of thermal infrared remote sensing data: Geological Society of America Abstracts with Programs, v. 26, no. 7, p. A89.
- Realmuto, V. J., 1990, Separating the effects of temperature and emissivity: Emissivity spectrum normalization, in Abbott, E. A., ed., *Proceedings, Second Annual Airborne Earth Science Workshop*, Volume 2: Jet Propulsion Laboratory Publication 90–55, p. 31–35.
- Realmuto, V. J., Hajek, P., Sinha, M. P., and Chrien, T. G., 1995, The 1994 laboratory calibration of TIMS, in Realmuto, V. J., ed., *Summaries, Fifth Annual Airborne Earth Science Workshop*, Volume 2: Jet Propulsion Laboratory Publication 95–1, p. 25–28.
- Reheis, M. C., and Kihl, R., 1995, Dust deposition in southern Nevada and California, 1984–1989: Relations to climate, source area, and lithology: *Journal of Geophysical Research*, v. 100, p. 8893–8918.
- Rendell, H. M., and Sheffer, N. L., 1996, Luminescence dating of sand ramps in the eastern Mojave Desert: *Geomorphology*, v. 17, p. 167–186.
- Ruff, S., Christensen, P. R., Barbera, P. W., and Anderson, D. L., 1997, Quantitative thermal emission spectroscopy of minerals: A laboratory technique for measurement and calibration: *Journal of Geophysical Research*, v. 102, p. 14899–14913.
- Sharp, R. P., 1966, Kelso Dunes, Mojave Desert, California: Geological Society of America Bulletin, v. 77, p. 1045–1074.
- Shipman, H., and Adams, J. B., 1987, Detectability of minerals on desert alluvial fans using reflectance spectra: *Journal of Geophysical Research*, v. 92, p. 10391–10402.
- Smith, R. S. U., 1984, Eolian geomorphology of the Devils Playground, Kelso Dunes and Silurian Valley, California, in Dohrenwend, J. C., ed., *Surficial geology of the eastern Mojave Desert, California*: Boulder, Colorado, Geological Society of America 1984 Annual Meeting field trip guidebook 14, p. 162–173.
- Thomson, J. L., and Salisbury, J. W., 1993, The mid-infrared reflectance of mineral mixtures (7–14 μm): *Remote Sensing of the Environment*, v. 45, p. 1–13.
- Tucker, C. J., Newcomb, W. W., and Dregne, H. E., 1994, AVHRR data sets for determination of desert spatial extent: *International Journal of Remote Sensing*, v. 15, p. 3547–3456.
- Wells, S. G., and McFadden, L. D., 1987, Influence of late Quaternary climatic changes on geomorphic processes on a desert piedmont, eastern Mojave Desert, California: *Quaternary Research*, v. 27, p. 130–146.
- Wintle, A. G., Lancaster, N., and Edwards, S. R., 1994, Infrared stimulated luminescence (IRSL) dating of late Holocene aeolian sands in the Mojave Desert, California, USA: *The Holocene*, v. 4, no. 1, p. 74–78.
- Yeend, W., Dohrenwend, J. C., Smith, R. S. U., Goldfarb, R., Simpson, R. W., Jr., and Muntz, S. R., 1984, Mineral resources and mineral resource potential of the Kelso Dunes Wilderness Study Area (CDCA-250), San Bernardino County, California: U.S. Geological Survey Open-File Report 84-647, 19 p.

MANUSCRIPT RECEIVED BY THE SOCIETY AUGUST 14, 1997

REVISED MANUSCRIPT RECEIVED MARCH 23, 1998

MANUSCRIPT ACCEPTED APRIL 27, 1998